Mc Kearney, Patrick; Schäfer, Sören; Liu, Xiaolong; Paulus, Simon; Lebershausen, Ingo; Radfar, Behrad; Vähänissi, Ville; Savin, Hele; Kontermann, Stefan

Impact of Pulse Duration on the Properties of Laser Hyperdoped Black Silicon

Published in:
Advanced Photonics Research

DOI:
10.1002/adpr.202300281

Published: 01/06/2024

Document Version
Publisher's PDF, also known as Version of record

ADVANCED PHOTONICS RESEARCH
Open Access
www.adpr-journal.com

Impact of Pulse Duration on the Properties of Laser Hyperdoped Black Silicon

Patrick Mc Kearney, Sören Schäfer, Xiaolong Liu, Simon Paulus, Ingo Lebershausen, Behrad Radfar, Ville Vähänissi, Hele Savin, and Stefan Kontermann*

The impact of three different pulse durations (100 fs, 1, and 10 ps) on the formation of laser hyperdoped black silicon with respect to surface morphology, sub-bandgap absorptance, the sulfur concentration profile, and the effective minority carrier lifetime after Al_2O_3 surface passivation is investigated. The current flow behavior is compared through the hyperdoped layer by *I–V* measurements after hyperdoping with different pulse durations. For conditions that give the same absolute sub-bandgap absorptance, an increase in pulse duration from 100 fs to 10 ps results in a shallower sulfur concentration profile. Findings are explained by an increasing ablation threshold from 0.19 J cm^{-2} for a pulse duration of 100 fs to 0.21 J cm^{-2} for 1 ps and 0.34 J cm^{-2} for 10 ps. The formation of an equally absorbing layer with a shallower doping profile results in a reduction in contact and/or sheet resistance. Despite the higher local sulfur concentration, the samples show no decrease in carrier lifetime measured by quasi-steady-state photoconductance decay on Al_2O_3 surface-passivated samples. The investigation shows that longer pulses of up to 10 ps during laser hyperdoping of silicon result in advanced layer properties that promise to be beneficial in a potential device application.

1. Introduction

Hyperdoping by ultrashort laser pulses has emerged as a promising technique for surface microstructuring and simultaneously introducing dopants into silicon at high concentrations for tailoring its optoelectronic properties. In addition to increased absorptance by light-trapping structures,[1–4] absorptance in the sub-bandgap region can be obtained if the process is carried out in sulfur hexafluoride (SF_6) containing atmosphere.[5–8] These properties make the resulting material a promising candidate for silicon-based infrared photodetectors, especially when the silicon crystal properties allow for excess carrier generation.[9,10]

The surface morphology and the absorptance strongly depend on the pulse density and peak fluence during the laser process.[10–12] Although surface patterning[13,14] and hyperdoping[15–18] have been shown to be achievable with pulse durations in the nanosecond, picosecond, and femtosecond range, only a few studies have been published on the effect of pulse duration on the surface structures, optical absorptance, and the doping profile. Her et al. showed that for constant laser fluence, pulse density, and wavelength, the distance between microstructures decreases continuously when the pulse duration is increased from 100 fs to 1 ps.[4] A further increase above 1 ps leads to an increase in the distance. Crouch et al. studied the surface and optical properties of hyperdoped black silicon prepared with 100 fs and 25 ns pulses.[15] The results show that ns pulses lead to higher absorptance and larger surface structures. However, in that study, there are large differences in the wavelength, pulse density, and fluence, making it difficult to draw conclusions about the influence of pulse duration alone. Zorba et al. investigated the properties after processing at 500 fs, 5 ps, and 15 ns at constant wavelength.[16] The statement that longer pulses lead to larger structures and higher absorptance is in good agreement with the results of another study.[15] Nevertheless, for each pulse duration, different combinations of pulse density and fluence were used in another study,[16] which again complicate the statement about the influence of the pulse duration on the material properties.

In this article, we report on the impact of pulse duration in the range from 100 fs to 10 ps on the fabrication of hyperdoped black silicon using one laser system at a constant wavelength of 1030 nm and expose all samples to a pulse density of 500 pulses per spot. By varying the fluence in the same range for different pulse durations, we investigate the interaction of these two parameters on the optical properties as well as the surface morphology. Based on this, we fabricate samples with pulse durations of 100 fs, 1, and 10 ps that exhibit a comparable surface morphology and sub-bandgap absorptance to investigate the effect of pulse duration on the doping profile, the current–voltage behavior, and the effective minority carrier lifetime.

P. Mc Kearney, S. Schäfer, S. Paulus, I. Lebershausen, S. Kontermann
Institute for Microtechnologies (IMtech)
University of Applied Sciences RheinMain
Am Brückweg 26, 65428 Rüsselsheim, Germany
E-mail: patrick.mckearney@hs-rm.de

X. Liu, B. Radfar, V. Vähänissi, H. Savin
Department of Electronics and Nanoengineering
Aalto University
Tietotie 3, FI-02150 Espoo, Finland

The ORCID identification number(s) for the author(s) of this article can be found under https://doi.org/10.1002/adpr.202300281.

DOI: 10.1002/adpr.202300281

2. Results and Discussion

2.1. Interaction of Pulse Duration and Peak Fluence

Figure 1 shows the square of the measured ablation diameter as a function of peak fluence for the pulse durations 100 fs, 1, and 10 ps with the corresponding fit functions. Extrapolation toward the *x*-axis yields the ablation threshold fluences 0.19, 0.21, and 0.34 J cm^{-2} for the respective pulse durations.[19] From the slope of the fit function, we determine the $1/e^2$ diameters, which are 60 µm for 100 fs, 72 µm for 1 ps, and 74 µm for 10 ps. This is in good agreement with the diameters measured with the camera-based beam profiling system which are 63 ± 5.1 µm for 100 fs and 70 ± 5.1 µm for 1 and 10 ps.

We use the determined ablation thresholds for the processing parameters in this work ($\lambda = 1030$ nm, $f_{rep} = 200$ kHz, pulse duration 0.1–10 ps, number of pulses $N = 10$) to classify the results during the discussion. The ablation threshold increases with increasing pulse duration due to decreasing intensity, which is in good accordance with literature.[2,20–23] Compared to previously published data[24–26] using similar parameters which are shown in **Table 1**, the values for the ablation thresholds determined here tend to be lower. Simultaneously the values reported here are an order of magnitude higher than those reported in another study.[27] We attribute this to the deviations in pulse duration and number[28] as well as repetition rate[29] in our experiments and thus consider the values to be reasonable.

We investigate the surfaces of samples prepared with the pulse durations 100 fs, 1, and 10 ps and peak fluences between 0.3 and 1.6 J cm^{-2} with an scanning electron microscope (SEM). For all pulse durations, we observe the formation of periodic, cone-like surface structures, whose diameter and height increase with the peak fluence whereas the area density decreases. **Figure 2**a–l shows that at constant fluence, the pulse durations 100 fs and 1 ps result in the same microstructured surfaces. For fluences below 1.0 J cm^{-2}, we observe an influence of the pulse duration when it is increased from 1 to 10 ps. We quantify the mean cone radius of the structures by calculating the radial autocorrelation function of the top-view SEM images and extract the first minimum in radial direction. **Figure 3** shows the results plotted versus the peak fluence.

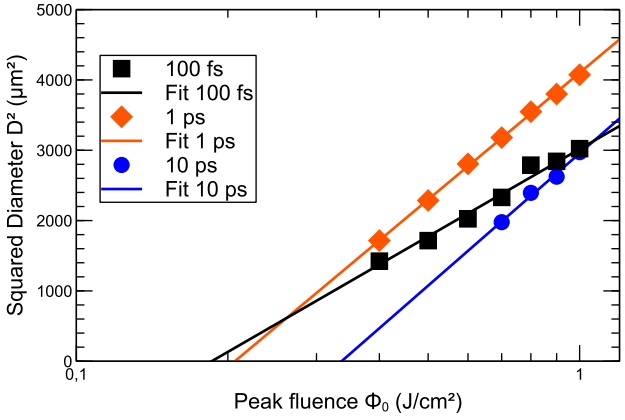

Figure 1. Squared ablation diameter plotted against the peak fluence for $N = 10$ pulses with pulse durations 100 fs, 1, and 10 ps. The intersection of the fit function with the *x*-axis yields the respective threshold fluence.

Table 1. Overview of ablation thresholds of silicon determined by Liu's method.

τ [ps]	λ [nm]	N	f_{rep} [kHz]	Φ_{Th} [J cm^{-2}]	References
12	1030	1	–	0.8, 1.68	[29]
0.38	1040	1	–	0.7	[28]
3	1030	–	1	0.43	[27]
10	1030	–	41 000	0.03	[31]
0.1	1030	10	200	0.19	This work
1	1030	10	200	0.21	This work
10	1030	10	200	0.34	This work

The mean radius of the surface structures increases for all pulse durations as the peak fluence increases. This behavior is in good accordance with previous studies on laser hyperdoping of silicon in SF6 atmosphere.[11,12,30] In the fluence range between 0.5 and 1.0 J cm^{-2}, the mean cone radius increases faster for both shorter pulser durations than for 10 ps pulses. In this fluence window, ten pulses result in smaller cone structures with a higher density. A similar behavior has been observed for a reduction from 5 ps to 500 fs.[16] Furthermore, it was reported that in the range from 100 fs to 15 ns, the radius of the light-trapping structures strongly depends on the pulse duration.[15,16] Furthermore, Figure 2m–p shows interconnections between directly adjacent microstructures. We attribute this observation to a longer melt time during the hyperdoping process due to the longer pulse duration. With a further increase in fluence, this effect is less pronounced, so that the influence of the pulse duration becomes less apparent.

Our findings show that for a given wavelength and pulse density, the combination of pulse duration and peak fluence determines the radius of the surface structures. Figure 3 shows that for fluences below 1.0 J cm^{-2}, for increasing pulse duration, higher fluences are required to obtain comparable surface structures, that is, comparable radii. Above 1.0 J cm^{-2}, the influence of pulse duration becomes negligible. Thus, comparable surface roughness can be produced in the investigated parameter space at different pulse durations.

Figure 4 shows the sub-bandgap absorptance at a wavelength of 1500 nm, plotted against the peak fluence. Since the absorptance is constant in the range from 1200 to 2500 nm, which is in good agreement with the work of Crouch et al.[31] this value is representative for the sub-bandgap absorptance. For all pulse durations, we observe in Figure 4 an increase in absorptance of the laser hyperdoped silicon samples with increasing fluence, which is attributed to stronger light trapping and a higher sulfur dose incorporated into the silicon lattice.[32] This absorptance saturates at a maximum value of 95%$_{abs}$.

While the absorptance curves for the pulse durations 100 fs and 1 ps are comparable within the error margin of 1%$_{abs}$, we observe that for a pulse duration of 10 ps, the absorptance changes less with increasing fluence. We attribute this to the fact that the size of the surface structures changes less with fluence the longer the pulses are, as shown in Figure 3. Therefore, the

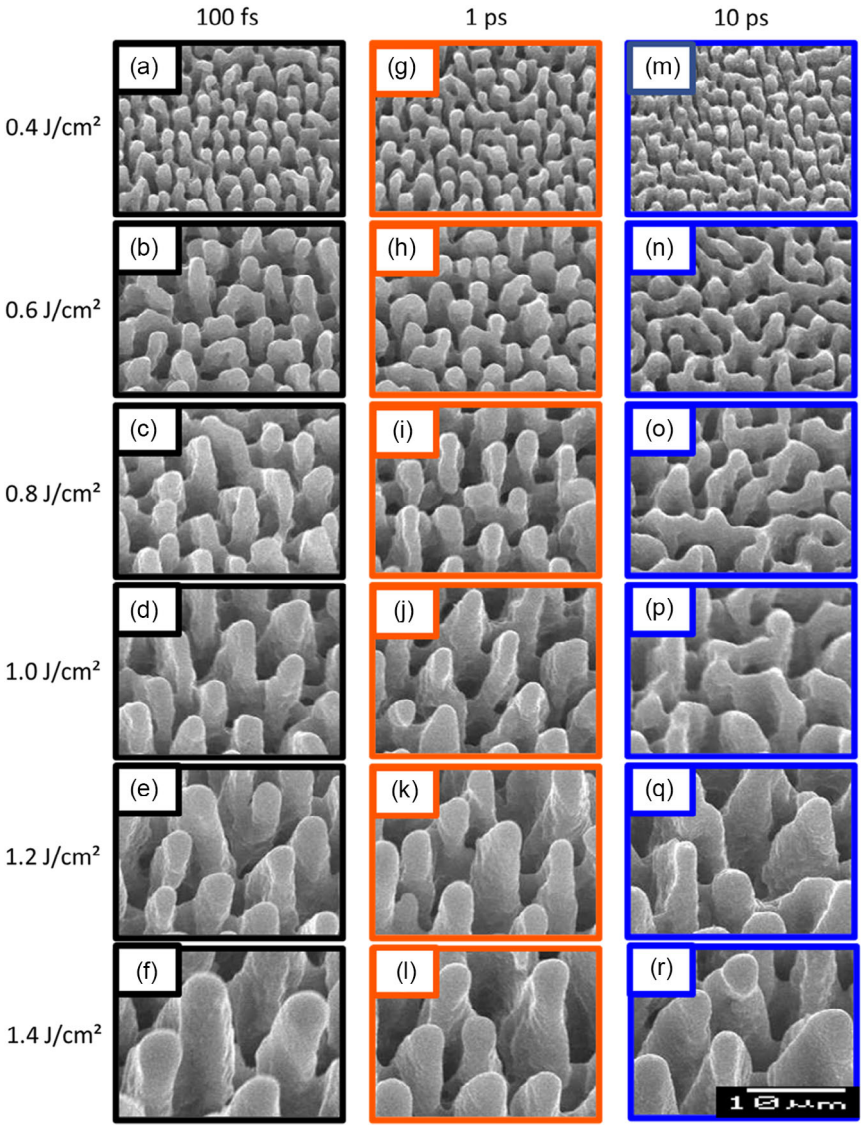

Figure 2. SEM micrographs of hyperdoped black silicon surfaces processed with fluences from 0.4 to 1.4 J cm^{-2} and a pulse duration of a–f) 100 fs, g–l) 1 ps, and m–r) 10 ps with a viewing angle of 30° to the surface.

light-trapping effect of the microstructures processed at the same peak fluence is less pronounced. To verify the cause for the difference in absorptance, we determine the optical thickness of the samples using the optical model of Schäfer et al.[12] The optical thickness is equal to the product of the absorption coefficient and the thickness of the absorbing layer which allows us to compare the absorptance of the samples independently of the surface reflectance. The optical thickness as a function of peak fluence is independent of the pulse duration. This means that the reduced absorptance for samples processed with 10 ps and peak fluences below 1.0 J cm^{-2} results from an increase in surface reflectance.

Previous work has shown strong influences of pulse duration on the achievable absorptance. Hyperdoping with femtosecond and picosecond pulses led to comparable results and an absorptance between 80%$_{abs}$ and 90%$_{abs}$, whereas an absorptance of 95%$_{abs}$ was reported when using nanosecond pulses. Compared to previous works,[15,16] we perform all experiments on a single-laser system and keep the wavelength and pulse density constant. The absorption measurements presented here show that the pulse duration plays a minor role in the achievable absorptance. By adjusting the peak fluence and thus the ratio of peak-to-threshold fluence, sub-bandgap absorptances of 95%$_{abs}$ can be achieved with pulses of length 100 fs, 1, and 10 ps, respectively. The results show that the pulse duration does not determine the surface roughness and optical absorptance, but rather dictates the fluence regime in which certain optical and surface structural properties can be achieved. Furthermore, we showed that the use of longer pulses has the advantage that this fluence regime becomes larger, which makes the process less sensitive to deviations in the pulse energy or the focus position.

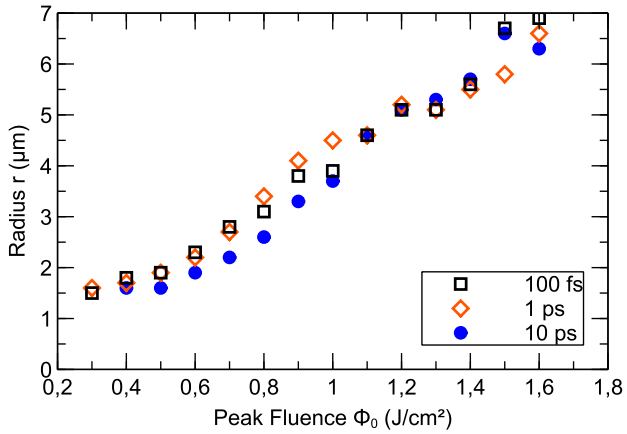

Figure 3. Mean cone radius plotted against the peak fluence for samples processed at 100 fs, 1, and 10 ps.

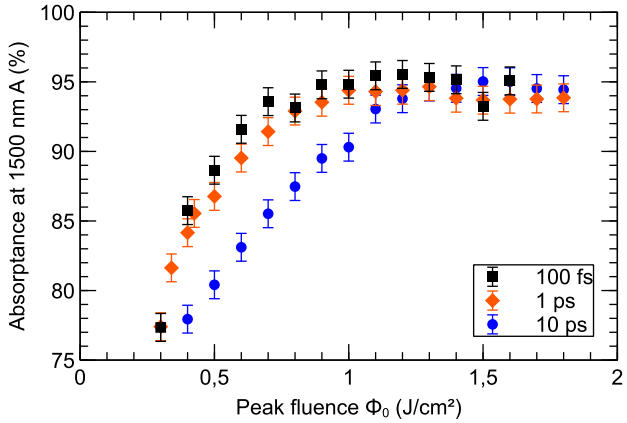

Figure 4. Sub-bandgap absorptance at 1500 nm plotted against the peak fluence for samples processed at 100 fs, 1, and 10 ps.

2.2. Impact of Pulse Duration

As for longer pulses, a higher fluence is required to achieve the maximum sub-bandgap absorptance, and we decide to compare the samples with 1.2 J cm^{-2} for 100 fs and 1 ps and 1.4 J cm^{-2} for 10 ps in the following sections. As these samples are comparable in cone radius (Figure 3) and absolute absorptance (Figure 4), we assume a comparable level of surface texturing and neglect any influence that could be traced back to a different morphology. Thus, we can study the pure impact of the pulse duration on the hyperdoped layer.

Figure 5 shows the measured sulfur concentration depth profiles of samples processed with pulse durations of 100 fs, 1, and 10 ps and peak fluences of 1.2, 1.2, and 1.4 J cm^{-2} respectively. These parameters assure comparability and account for the fact that the profiles are measured on a rough and randomly structured surface, which must be considered when interpreting the profiles. Since the depth is calculated from the measured sputtering rate on a planar reference and the sputtering rate depends on the angle of incidence of the ion beam,[30,33] the surface structures may result in a systematic error for the measurement of the

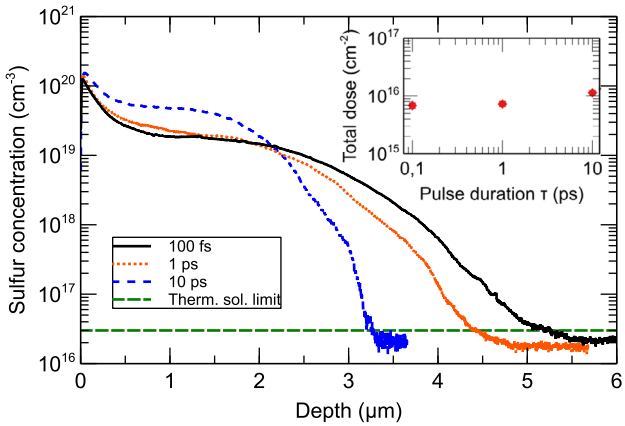

Figure 5. SIMS profiles of samples which have been hyperdoped with 100 fs at 1.2 J cm^{-2} (black), 1 ps at 1.2 J cm^{-2} (orange), and 10 ps at 1.4 J cm^{-2} (blue). The green dashed line indicates the thermal solubility limit of sulfur in silicon at 3×10^{16} cm^{-3}. The inset shows the total dose of the corresponding samples.

depth. For this reason, the absolute depths may deviate from the measured depths. Nevertheless, since the surface roughness of the investigated samples is comparable, we assume that this systematic error is for these samples. In addition, the peaks of the cone structures, which have a higher sulfur concentration than the valleys, are preferentially ablated at the beginning. Due to the size of the ion beam, such local differences cannot be resolved, which is why the measured sulfur concentration is taken as an average over the area of the ion beam.

The surface concentration is above 10^{20} cm^{-3} for all samples and the maxima are located within the first 100 nm from the surface. Further on, the concentration decreases with increasing distance from the surface for all samples. Within the first 2 µm from the surface, the concentration of the sample processed with 10 ps pulse duration is higher than that of the other samples, which are on a similar level. From this point, the concentration of all samples starts to decrease. The concentration reaches the thermal solubility limit of 3×10^{16} cm^{-3}[34] at 3.25, 4.40, and 5.20 µm from the surface and the total dose, that is, the integral over the depth, is equal to $(1.1 \pm 0.03) \times 10^{16}$ cm^{-2}, $(7.3 \pm 0.2) \times 10^{15}$ cm^{-2}, and $(6.9 \pm 0.2) \times 10^{15}$ cm^{-2} for the samples processed with 10, 1 ps, and 100 fs respectively.

The fabricated samples exhibit a maximum sulfur concentration of 1.5×10^{20} cm^{-3} (0.3 at%), which decreases with distance from the surface. The measured maxima are in the same order of magnitude reported by Crouch et al.[31] In the work of Guenther et al. and Lin et al. peak concentrations of 5.0×10^{19} cm^{-3} (0.1 at%)[35] and 2.0×10^{18} cm^{-3} (0.004 at%)[36] were reported, but lower pulse densities were used here.

We measure a doping depth of up to 6 µm, which is a higher value compared to previously reported values of some tens[36] and hundreds[37] of nanometers up to a micrometer,[35] depending on hyperdoping process and parameters. We attribute this partly to the high pulse density used in this work and partly to the systematic error of the measurement due to the surface roughness, which both result in a higher doping depth.

We observe that the doping depth decreases with increasing pulse duration. We attribute this to the fact that the melting

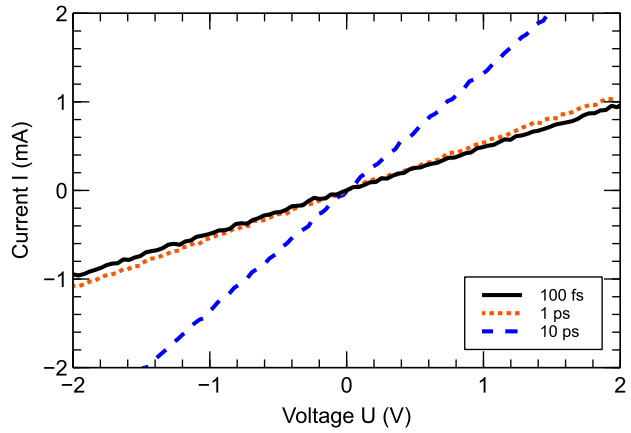

Figure 6. Current–voltage measurement across the hyperdoped layer of samples which have been processed with 100 fs at 1.2 J cm^{-2} (black), 1 ps at 1.2 J cm^{-2} (orange), and 10 ps at 1.4 J cm^{-2} (blue).

depth scales with the logarithm of the ratio of peak to melting fluence in analogy to the ablation depth.[38] For the parameters studied here, this ratio is 6.3, 5.7, and 4.1 for the samples prepared at 100 fs, 1, and 10 ps, respectively. Since the optical absorptance and the surface morphology of these samples are comparable, we have shown that the pulse duration is a parameter for controlling the thickness of the hyperdoped layer.

Figure 6 shows the current–voltage measurement of the samples when placing probes on the two contact pads on top, so that the current flows exclusively through the hyperdoped layer. Due to the surface roughness, the actual layer thickness is less than 300 nm since it was calculated from the deposition rate for a planar substrate. As the current increases linearly with the voltage for all samples, the layer thickness is still high enough to achieve Ohmic contacts. The 100 fs and 1 ps samples show a similar behavior, whereas the slope rises when increasing the pulse duration to 10 ps. The reciprocal of the slope of the curves yields resistances of 2062, 1838, and 740 Ω for 100 fs, 1, and 10 ps, respectively. Thus, the 10 ps sample exhibits a lower contact resistance and/or a higher conductivity, but this measurement does not allow us to distinguish between the two quantities. Since the surface concentrations in Figure 5 are comparable, the contact resistance should be of the same order of magnitude for all samples. This suggests that the differences are due to higher conductivity. However, this needs to be verified by measuring the contact resistance. Nevertheless, since a low contact resistance and transverse conductivity are typically beneficial in the application in an optoelectronic device, hyperdoping with longer pulse durations seems to be advantageous.

Figure 7 shows the injection level-dependent effective charge carrier lifetime measured in the hyperdoped samples. As mentioned before, we have used high-quality substrates and applied very effective atomic layer deposition (ALD) Al_2O_3 surface passivation to mitigate both bulk and surface recombination. Therefore, the effective lifetime here can be considered as a direct figure of merit for the laser hyperdoping process-induced defects and related recombination. At the injection level of $\Delta n = 10^{15}$ cm^{-3}, the measured lifetimes are ≈9 µs. At higher injection levels we do not see any significant differences between the obtained values for the different pulse durations. Looking at the values more closely, the measured lifetime seems to slightly increase when the pulse duration increases. Due to the small magnitude of the difference, it is however impossible to fully rule out measurement uncertainty as one possible explanation for this trend.

All samples show signs of carrier trapping, as can be seen by an increasing lifetime toward lower injection levels.[39,40] A steeper increase of the 10 ps sample may point to a different type or concentration of trapping centers. However, as the results indicate, a longer pulse duration does not result in a more recombinative active hyperdoped layer.

In the literature the low lifetime after the laser hyperdoping process is linked to two causes. The work of Liu et al. shows that the crystal damage caused by the laser process strongly reduces the carrier lifetime and reaches several micrometers into the substrate.[41] Furthermore, the optical-pump/terahertz-probe measurements of Sher et al. show that the carrier lifetime decreases with increasing sulfur concentration and is below a few hundred picoseconds within the hyperdoped layer.[42] This is attributed to the greatly increased recombination caused by the sulfur defect levels within the bandgap. Since the sulfur concentration in all our samples here is in the same order of magnitude, we do not expect any related significant differences in effective lifetime.

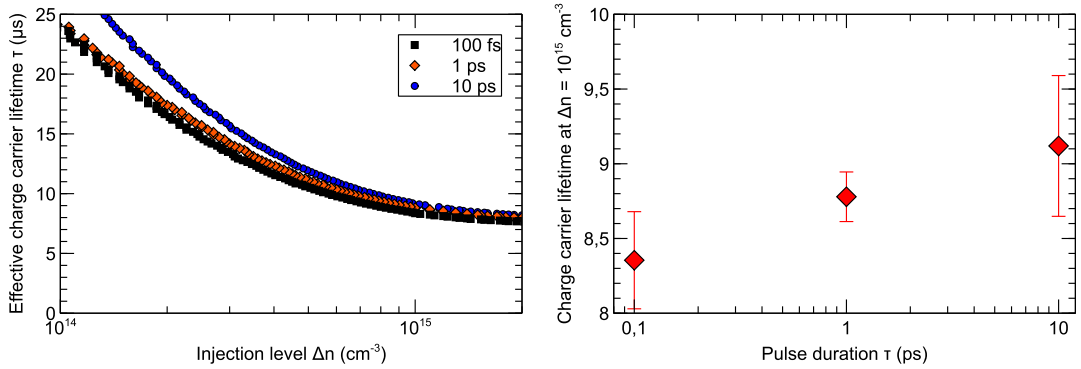

Figure 7. Left: Injection level-dependent effective charge carrier lifetime measured by QSSPC. Right: Effective charge carrier lifetime at an injection level of 10^{15} cm^{-3} plotted against the pulse duration.

3. Conclusion

We have investigated the influence of the interaction of peak fluence and pulse duration in the range of 100 fs–10 ps during laser hyperdoping of sulfur in silicon on the resulting optoelectronic properties. Our results show that similar surface morphologies and subbandgap absorptance can be obtained using different pulse durations. Due to the pulse length dependence of the threshold fluence, the fluence range in which comparable properties are achieved shifts to higher fluences with increasing pulse duration. Furthermore, it was shown that the doping profile, in particular the thickness of the hyperdoped layer, is smaller with higher pulse duration, which results in a lower contact and/or sheet resistance. Minority carrier lifetime measurements on surface-passivated samples indicate a comparable effective lifetime at an injection level of 10^{15} cm^{-3} for all pulse durations. In summary, it was shown that the pulse duration is an important processing parameter for optimizing material parameters with respect to optoelectronic applications.

4. Experimental Section

We irradiated double-side-polished 2″ and 4″ Czochralski grown *p*-type silicon (100) wafers with a specific resistivity of 1–10 Ω cm with ultrashort laser pulses with different pulse durations in ambient air to determine the ablation threshold fluence by D-squared method[19] and in sulfur hexafluoride (SF6) atmosphere to fabricate hyperdoped black silicon. The Yb:YAG laser source (Amplitude Tangor 100) emitted pulses with a pulse duration of 800 fs at the central wavelength 1030 nm with a repetition rate of 200 kHz, which could be chirped up to 1 and 10 ps by adjusting the compressor and shortened to 100 fs by an optical compression module (Amplitude Compress 10). The pulse duration in the processing plane was measured with an autocorrelator. The output pulse energy of the laser source was controlled with an acousto-optical modulator and that of the compression module with an attenuator consisting of a half-wave plate and a polarizing beam splitter.

The laser pulses passed through a scanning system consisting of a two-axis galvanometer scanner and were focused by an F-Theta objective with a focal length of 340 mm onto the wafer surface inside a processing chamber. The $1/e^2$ beam diameter in the focal plane was measured with a camera-based beam profiling system. The peak fluence was controlled by adjusting the pulse energy.

For determining the ablation threshold fluence, we irradiated the samples with 10 pulses per spot at different fluences and pulse durations and measured the ablation diameter with a digital light microscope (Keyence VHX-7000 series).

For laser hyperdoping, we mounted the wafers into a vacuum chamber with a diameter of 15 cm and a total height of 30 cm which was sealed on top with a fused silica window. We evacuated the chamber to 1 mbar with a rotary vane pump and refilled it with sulfur hexafluoride to a pressure of 675 mbar. To maintain a stable and constantly regenerated process atmosphere, the SF6 flow was set to 100 sccm with a mass flow controller and the exhaust was controlled with a needle valve. The laser pulses were scanned across the wafer surface with a pulse overlap of 96% in both, scanning direction and perpendicular to it. The total number of pulses per spot area was 500. After fabrication, we cleaned the samples in solvents (acetone, isopropanol, and DI water).

We investigated the surface morphology with a scanning electron microscope (JEOL JSM-6380LV) operating at 10 kV acceleration voltage and a viewing angle of 0° and 30°.

We characterized the optical properties of the samples with a spectrophotometer (Perkin Elmer Lambda750) with an integrating sphere by measuring the reflectance R and transmittance T in the spectral range from 250 to 2500 nm. The absorptance A was calculated by $A = 1 - R - T$.

We measured the sulfur doping concentration profile of samples processed with different pulse durations with a secondary-ion mass spectrometer (SIMS) (Cameca ims 4f-E6) using 14.5 keV Cs+ ions. The measured sulfur concentration was calibrated with a planar Si:S implantation standard. The crater dimension was 50 by 50 µm and the depth was measured by the sputtering rate on the calibration sample.

We investigated the current–voltage characteristics across the hyperdoped layer of samples which were processed on *p*-type float zone grown wafers (100) with a resistivity of 2000–8000 Ω cm. After laser processing, we cleaned the samples in solvents (acetone, isopropanol, and DI water) and performed hydrofluoric acid (HF) dip (1% HF solution, 5 min) to remove the native surface oxide. We deposited two circular aluminum contacts with 1 mm in diameter and 300 nm in thickness through a shadow mask on the hyperdoped silicon surface by magnetron sputtering and thermally annealed the samples after metal deposition on a hot plate in air at 400 °C for 1 min. We measured the current while applying voltages from −2 to 2 V.

To be able to directly probe the possible effect of the laser pulse duration on the achievable minority carrier lifetime, in addition to using high-quality substrates to mitigate bulk recombination, we also mitigated surface recombination by applying ALD Al_2O_3 surface passivation[43–45] prior to characterizing the effective minority carrier lifetime. First, the samples were cleaned with solvents (acetone, isopropanol, and DI water) and the standard radio corporation of America (RCA) cleaning sequence. Then, Al_2O_3 deposition was performed on both sides of the wafers in a Beneq TFS-500 ALD reactor for 500 cycles at 200 °C with trimethylaluminium (TMA) and H_2O as precursors. After ALD, the passivation was activated by a postdeposition anneal in forming gas at 400 °C for 30 min. The effective minority carrier lifetime as a function of injection level was then measured using the quasi-steady-state-photoconductance (QSSPC) technique with a Sinton WCT-120 lifetime tester.

Acknowledgements

This work was funded by the Federal Ministry of Education and Research of Germany under grant no. FKZ 03INT701AA and by Business Finland through the "FemtoBlack" project under grant no. 7479/31/2019. S.S. acknowledges funding by the German Federal Ministry of Education and Research in the context of the federal state program "FH-Personal" under the grant no. 03FHP147A (REQUAS). X.L. acknowledges the financial support of the Academy of Finland (#354199). B.R. and V.V. acknowledge the financial support of the Academy of Finland (#331313). The work was related to the Flagship on Photonics Research and Innovation "PREIN" funded by Academy of Finland. The authors acknowledge the provision of facilities and technical support by Micronova Nanofabrication Centre in Espoo, Finland, within the OtaNano research infrastructure at Aalto University. The authors would also like to acknowledge Professor Dr. Markus Bender and his team for providing the opportunity of using the scanning electron microscope and Professor Dr. Jutta Kerpen and her team for providing the opportunity of using the digital light microscope.

Conflict of Interest

The authors declare no conflict of interest.

Data Availability Statement

The data that support the findings of this study are available from the corresponding author upon reasonable request.

Keywords

atomic layer depositions, black silicon, doping profiles, pulse durations, ultrashort pulse laser hyperdoping

Received: October 2, 2023
Revised: February 16, 2024
Published online:

[1] J. E. Sipe, J. F. Young, J. S. Preston, H. M. van Driel, *Phys. Rev. B* **1983**, *27*, 1141.
[2] J. Bonse, S. Baudach, J. Krüger, W. Kautek, M. Lenzner, *Appl. Phys. A* **2002**, *74*, 19.
[3] T.-H. Her, R. J. Finlay, C. Wu, S. Deliwala, E. Mazur, *Appl. Phys. Lett.* **1998**, *73*, 1673.
[4] T.-H. Her, R. J. Finlay, C. Wu, E. Mazur, *Appl. Phys. A* **2000**, *70*, 383.
[5] C. Wu, C. H. Crouch, L. Zhao, J. E. Carey, R. Younkin, J. A. Levinson, E. Mazur, R. Farrell, P. Gothoskar, A. Karger, *Appl. Phys. Lett.* **2001**, *78*, 1850.
[6] B. Franta, E. Mazur, S. K. Sundaram, *Int. Mater. Rev.* **2018**, *63*, 227.
[7] J. M. Warrender, *Appl. Phys. Rev.* **2016**, *3*, 31104.
[8] A. L. Baumann, K.-M. Guenther, P. Saring, T. Gimpel, S. Kontermann, M. Seibt, W. Schade, *Energy Procedia* **2012**, *27*, 480.
[9] S. Paulus, P. Mc Kearney, F. Völklein, S. Kontermann, *AIP Adv.* **2021**, *11*, 75014.
[10] K.-M. Guenther, T. Gimpel, J. W. Tomm, S. Winter, A. Ruibys, S. Kontermann, W. Schade, *Appl. Phys. Lett.* **2014**, *104*, 042107.
[11] J. E. Carey, C. H. Crouch, M. Shen, E. Mazur, *Opt. Lett.* **2005**, *30*, 1773.
[12] S. Schäfer, P. McKearney, S. Paulus, S. Kontermann, *J. Appl. Phys.* **2022**, *131*, 243102.
[13] X. N. Zhu, H. L. Zhu, D. W. Liu, Y. Huang, X. Wwang, H. Yu, S. Wang, X. Lin, P. Han, *Adv. Mater. Res.* **2011**, *418–420*, 217.
[14] A. J. Pedraza, J. D. Fowlkes, D. H. Lowndes, *Appl. Phys. Lett.* **1999**, *74*, 2322.
[15] C. H. Crouch, J. E. Carey, J. M. Warrender, M. Aziz, E. Mazur, F. Génin, *Appl. Phys. Lett.* **2004**, *84*, 1850.
[16] V. Zorba, N. Boukos, I. Zergioti, C. Fotakis, *Appl. Opt.* **2008**, *47*, 1846.
[17] S. Hu, P. Han, S. Wang, X. Mao, X. Li, L. Gao, *Semicond. Sci. Technol.* **2012**, *27*, 102002.
[18] P. Saring, A. Lena Baumann, B. Schlieper-Ludewig, S. Kontermann, W. Schade, M. Seibt, *Appl. Phys. Lett.* **2013**, *103*, 061904.
[19] J. M. Liu, *Opt. Lett.* **1982**, *7*, 196.
[20] B. C. Stuart, M. D. Feit, A. M. Rubenchik, B. W. Shore, M. D. Perry, *Phys. Rev. Lett.* **1995**, *74*, 2248.
[21] M. Lenzner, J. Krüger, S. Sartania, Z. Cheng, C. Spielmann, G. Mourou, W. Kautek, F. Krausz, *Phys. Rev. Lett.* **1998**, *80*, 4076.
[22] H. O. Jeschke, M. E. Garcia, M. Lenzner, J. Bonse, J. Krüger, W. Kautek, *Appl. Surf. Sci.* **2002**, *197–198*, 839.
[23] J. Byskov-Nielsen, J.-M. Savolainen, M. S. Christensen, P. Balling, *Appl. Phys. A* **2010**, *101*, 97.
[24] J. Thorstensen, S. E. Foss, *J. Appl. Phys.* **2012**, *112*, 103514.
[25] R. Moser, M. Domke, J. Winter, H. P. Huber, G. Marowsky, *Adv. Opt. Technol.* **2018**, *7*, 255.
[26] Y.-H. Liu, C.-W. Cheng, *J. Manuf. Mater. Process.* **2023**, *7*, 68.
[27] P. Mc Kearney, S. Schäfer, S. Paulus, M. Roser, F. Piermaier, I. Lebershausen, S. Kontermann, *J. Appl. Phys.* **2023**, *133*, 13102.
[28] C. S. R. Nathala, A. Ajami, W. Husinsky, B. Farooq, S. I. Kurdyashov, A. Daskalova, I. Bliznakova, A. Assion, *Appl. Phys. A* **2016**, *122*, 107.
[29] J. Schille, R. Ebert, U. Loeschner, P. Scully, N. Goddard, H. Exner, in *Proc. SPIE Int. Soc. Opt. Eng.*, SPIE, USA **2010**, p. 758915.
[30] N. Gosset, M. Boufnichel, E. Bahette, W. Khalfaoui, R. Ljazouli, V. Grimal-Perrigouas, R. Dussart, *J. Micromech. Microeng.* **2015**, *25*, 95011.
[31] C. H. Crouch, J. E. Carey, M. Shen, E. Mazur, F. Génin, *Appl. Phys. A* **2004**, *79*, 1635.
[32] M.-J. Sher, E. G. Hemme, *Semicond. Sci. Technol.* **2023**, *38*, 33001.
[33] L. Frey, C. Lehrer, H. Ryssel, *Appl. Phys. A* **2003**, *76*, 1017.
[34] R. O. Carlson, R. N. Hall, E. M. Pell, *J. Phys. Chem. Solids* **1959**, *8*, 81.
[35] K.-M. Guenther, T. Gimpel, S. Kontermann, W. Schade, *Appl. Phys. Lett.* **2013**, *102*, 202104.
[36] Y.-T. Lin, N. Mangan, S. Marbach, T. Schneider, G. Deng, S. Zhou, M. Brenner, E. Mazur, *Appl. Phys. Lett.* **2015**, *106*, 062105.
[37] C. B. Simmons, A. J. Akey, J. P. Mailoa, D. Recht, M. Aziz, T. Buonassisi, *Adv. Funct. Mater.* **2014**, *24*, 2852.
[38] C. Momma, S. Nolte, B. N. Chichkov, F. V. Alvensleben, A. Tünnermann, *Appl. Surf. Sci.* **1997**, *109–110*, 15.
[39] D. Macdonald, A. Cuevas, *Appl. Phys. Lett.* **1999**, *74*, 1710.
[40] D. Macdonald, R. A. Sinton, A. Cuevas, *J. Appl. Phys.* **2001**, *89*, 2772.
[41] X. Liu, B. Radfar, K. Chen, E. Pälikkö, T. Pasanen, V. Vähänissi, H. Savin, *IEEE Photonics Technol. Lett.* **2022**, *34*, 870.
[42] M.-J. Sher, C. B. Simmons, J. J. Krich, A. Akey, M. Winkler, D. Recht, T. Buonassisi, M. Aziz, A. Lindenberg, *Appl. Phys. Lett.* **2014**, *105*, 053905.
[43] B. Hoex, J. J. H. Gielis, M. C. M. van de Sanden, W. Kessels, *J. Appl. Phys.* **2008**, *104*, 113703.
[44] P. Repo, A. Haarahiltunen, L. Sainiemi, M. Yli-Koski, H. Talvitie, M. Schubert, H. Savin, *IEEE J. Photovolt.* **2013**, *3*, 90.
[45] X. Liu, B. Radfar, K. Chen, T. Pasanen, V. Vähänissi, H. Savin, *Adv. Photonics Res.* **2022**, *3*, 2100234.